Investigating the Impact of Magnetic Fields and Pulsating Pressure on Non-Newtonian Fluid Flow in Symmetric/Asymmetric Corrugated Microchannels

Ahmed Y. Sayed [a], Shaaban I. Ahmed [*, b], Khaled. S. Mekheimer [c] and Mohamed S. Abdel-wahed [b, d]

[a] Department of Engineering Mathematics and Physics, Faculty of Engineering El-Materia, Helwan University, Cairo, Egypt.
[b] Department of Basic Engineering Sciences, Faculty of Engineering, BADR University in Cairo BUC, Egypt
[c] Department of Mathematics, Faculty of Science (Boys), Al-Azhar University, Cairo, Egypt.
[d] Department of Basic Engineering Sciences, Faculty of Engineering at Benha, Benha University, Cairo, Egypt.

Abstract

This study presents approximate analytical solutions for the velocity and volume flow rate of an electrically conducting, incompressible, and viscous Jeffrey fluid flowing through an asymmetric corrugated channel between two slit microparallel plates under electromagnetohydrodynamic conditions. The study uses the perturbation method to describe the periodic sinusoidal waves with small amplitude that characterize the corrugations of the two walls, which can be either in phase or half-period out of phase. The study also examines how the corrugations affect the velocity of the EMHD flow by performing numerical computations. The results show the dependence of the velocity profiles and mean velocity parameter on various factors, including Reynolds number (Re), Hartmann number (Ha), Porous Medium (Da) , dimensionless wave number (λ) of the wall perturbation, and the dimensionless relaxation time (λ_1) and retardation time(λ_2). The findings of this study have important implications for understanding the behavior of non-Newtonian fluids within asymmetric corrugated channels under electromagnetohydrodynamic conditions.

Keywords: Microchannel, Corrugated walls, Perturbation method, Jeffrey fluids, Nanofluid, Pulsating pressure.

1. Introduction.

Jeffery fluid is a type of non-Newtonian fluid that has gained significant importance in the field of fluid mechanics due to its unique properties. Unlike Newtonian fluids, which have a constant viscosity regardless of the applied stress, Jeffery fluids exhibit time-dependent viscosity that changes in response to the applied stress. This property makes them particularly useful in industrial processing, oil drilling, and biomedical engineering. The study of Jeffery fluid is crucial because it has the potential to revolutionize the way we approach fluid mechanics problems. Understanding the behavior of these fluids can lead to more efficient methods for processing materials, designing machinery, and treating medical conditions. The study of Jeffery fluid is an

***Corresponding Author Email:** shaban.Ebrahim@buc.edu.eg

active area of research, with ongoing discoveries and insights. As such, it is an exciting and dynamic field that has the potential to shape the future of many industries. [1-4]

This research focuses on fluid dynamics in microdevices, highlighting the significance of driving forces, geometry, and surface chemistry. It examines the interaction of physical phenomena such as pressure gradients, electrokinetics, and capillarity, and their effect on fluid flows in microfluidic devices. The study also explores new fluid dynamics problems and responses due to the unique geometries of these devices. Overall, this study contributes to our understanding of fluid dynamics in microfluidic devices and their applications in scientific and industrial contexts.

The feasibility of using electric and magnetic fields for EMHD micropumps has been demonstrated using both direct current and alternating current. [5-8] The research discussed in this context focuses on experimental investigations of turbulent flow over rough and smooth surfaces in the presence of an adverse pressure gradient. Tay et al. [9-11] conducted such investigations over two rough surfaces and a smooth surface, while Tsikata and Tachie [12-14] studied turbulent flows over smooth and rough walls in a channel driven by APG flow using experimental methods. Therefore, the common theme among these studies is the experimental examination of turbulent flow under adverse pressure gradient conditions.

In a recent study, Buren et al. [15] used the perturbation method to investigate the flow of EMHD Newtonian fluid through a micro parallel channel with corrugated walls, examining the effect of roughness on velocity and average velocity in detail. Roughness is commonly used in mechanical manufacturing and biomedical applications [16-17], where the fluids may not behave as Newtonian fluids. Additionally, the peristaltic flow of Jeffrey fluid was studied in a 3D rectangular duct and an asymmetric porous channel [18-20]. All the studies mentioned in this context focus on experimental investigations. However, Si and Jian [21] used the perturbation method to analytically solve the problem of Jeffrey fluid flow in a parallel microchannel with corrugated walls driven by Lorenz force. Additionally, Buren and Jian et al. [22-23] conducted an analytical study of Newtonian fluid flow in a parallel rough microchannel driven by pressure and Lorenz

force. It is noteworthy that there is currently no analytical solution available for fluid flow in a roughness channel driven by an oscillating pressure gradient.

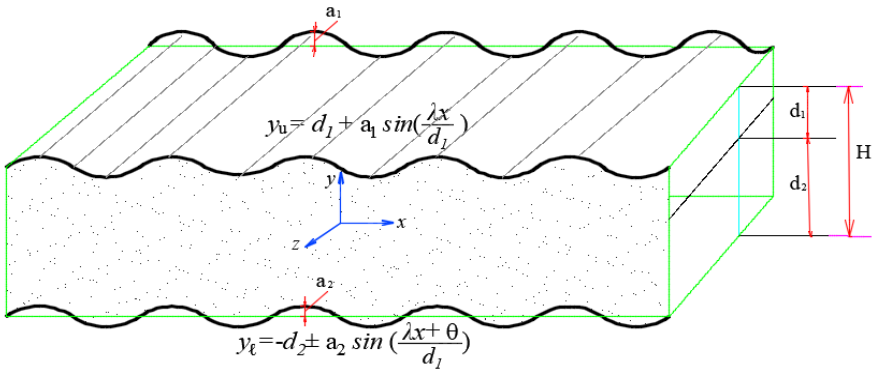

Figure 1. Geometry of the problem

2. Mathematical Model

This study investigates the electromagnetic hydrodynamic (EMHD) flow of an incompressible, electrically conducting Jeffrey fluid with density ρ and electrical conductivity σ, between two corrugated walls with a fixed height of H in a microchannel. The corrugated wall has an amplitude of 0.1H, representing a geometrical deformation in microchannels fabricated using precise manufacturing techniques. Figure (1) illustrates the layer thickness W, where $L \gg H$, and the orientation of the y, z, and x-axes. The upper and lower walls exhibit a corrugated wall, as defined in reference [24].

$$y_u^* = d_1^* + a_1^* \sin\left(\frac{\lambda\, x^*}{d_1}\right) \quad , \quad y_l^* = -d_2^* + a_2^* \sin\left(\frac{\lambda\, x^* + \theta^*}{d_1}\right), \tag{1}$$

where $a_1^* = \varepsilon\, d_1^*$, $a_2^* = \alpha\, a_1^*$, $d_2^* = \gamma\, d_1^*$. The flow is unsteady, laminar, and incompressible, occurring between two corrugated walls with a height of H. The layer thickness W is shown in Figure 1, with the y-axis perpendicular to the walls and the z

and x-axes tangential to the wall surface. The corrugated wall is defined in reference [24], with the amplitude of the waves represented by a_1 and a_2, the wavelength by λ, and the width of the channel by $d_1 + d_2$. The phase difference between the two corrugated walls is denoted by θ^*. The continuity and momentum equations are derived for an incompressible fluid, as described in references [24-25] further.

a_1^*; a_2^*; d_1^*; d_2^* and / satisfies the condition $a_1^{*2} + a_2^{*2} + 2a_1^* a_2^* \cos\theta \leq (d_1^* + d_2^*)^2$

$$\nabla \cdot V = 0 \tag{2}$$

$$\rho_f \frac{\partial \vec{u}}{\partial t} + \rho_f (\vec{u} \cdot \nabla)\vec{u} = -\nabla \vec{p} + \mu_f \nabla \tau^* + \vec{F} \tag{3}$$

$$\vec{J} = \sigma\left(\vec{E} + \vec{V} \times \vec{B}\right) \tag{4}$$

In equation (4), $\vec{E}$ represent applied electric field, respectively. $\vec{F}$ represents the Lorentz force, which arises from the interaction between fluid flow and applied magnetic field, where the magnetic field acts in the y-direction as $\vec{B} = B_0 \vec{e}_y$, and the uniform electric field is $\vec{E} = E_x \vec{e}_x$. The electric current density $\vec{J}$ takes the form $\vec{J} = \sigma\left[\vec{u} \times \vec{B}\right] + \sigma\vec{E}$. Thus, the constitution relation of Jeffrey fluid [26-27] satisfies:

$$\tau_{ij}^* + \lambda_1 \frac{\partial \tau_{ij}^*}{\partial t^*} = \mu \left(\gamma_{ij}^* + \lambda_2 \frac{\partial \gamma_{ij}^*}{\partial t^*} \right). \tag{5}$$

Here $\gamma_{ij}^* = \frac{\partial u_j^*}{\partial x_i^*}$ and τ_{ij}^* represent the strain and stress tensors, respectively. denotes the zero shear rate viscosity, while λ_1 and λ_2 refer to the relaxation and retardation times, respectively. It is worth noting that in general, the retardation time λ_2 is smaller than the relaxation time λ_1 [27-28]. The no-slip boundary conditions dictate that the corresponding boundary conditions of equation (3) can be expressed as:

$$w^*(x^*, y_u^*) = w^*(x^*, y_l^*) = 0 \ . \tag{6}$$

If we set the relaxation time λ_1 and retardation time λ_2 to zero in equation (5), it becomes the constitutive relation for a Newtonian fluid. In this case, we can obtain an analytical solution for the Newtonian fluid, which can be used to validate the analytical solution for a Jeffrey fluid. The liquid flowing through the microchannel is assumed to be incompressible and flowing only in the z^* direction. Since the channel in thez^*

direction is assumed to be open, we can ignore pressure gradients along the microchannel [28]. The velocity $w^*(x^*, y^*, t^*)$ satisfies.

$$\left(1+\lambda_1\frac{\partial}{\partial t^*}\right)\left[\rho\frac{\partial w^*}{\partial t^*}+\frac{\partial \mathrm{P}}{\partial \mathrm{z}^*}+\sigma w^* B_o^2-\sigma E_x\, B_o-\frac{\mu}{k}w^*\right]$$
$$=\mu\left(1+\lambda_2\frac{\partial}{\partial t^*}\right)\left(\frac{\partial^2 w^*(x^*,y^*)}{\partial {x^*}^2}+\frac{\partial^2 w^*(x^*,y^*)}{\partial {y^*}^2}\right) \quad (7)$$

In the current analysis of EMHD flow, it is assumed that the velocity, w^*, k be the permeability of the porous medium and the electric field E_x, exhibit periodic behavior and can be mathematically represented using complex forms. Likewise, the pressure can also be represented in a similar fashion [29-30].

$$\frac{\partial \mathrm{P}}{\partial \mathrm{z}^*}=-\frac{\mu_f\,\omega\,k\,\cos\omega t^*}{H}=-\frac{\mu_f\,\omega\,\tau}{H}\Re\{e^{i\,\omega\,t^*}\} \quad (8)$$

$$\therefore w^*=\Re\{u^*(x^*,y^*)e^{i\,\omega\,t^*}\} \quad , \quad E_x=\Re\{E_0\,e^{i\,\omega\,t^*}\} \quad (9)$$

In the given equation, $\Re\{\}$ represents the real part of the function, ω is the imposed AC electric field's angular frequency, i is the imaginary unit, and w and E_0 denote the amplitudes of velocity and AC electric field, and τ are amplitudes of velocity and pressure gradient field. Upon substituting Eqs (8), (9) into Eq. (7), we obtain:

$$\left(\rho\left(i\,\omega e^{i\,\omega\,t^*}u^*(x^*,y^*)\right)-\frac{\mu\,\omega\,\tau}{d_1}e^{i\,\omega\,t^*}+\sigma\left(u^*(x^*,y^*)e^{i\,\omega\,t^*}\right)B_o^2-\sigma\left(E_0\,e^{i\,\omega\,t^*}\right)B_o\right.$$
$$-\frac{\mu}{k}\left(u^*(x^*,y^*)e^{i\,\omega\,t^*}\right)$$
$$+\lambda_1\frac{\partial}{\partial t^*}\left(\rho\left(i\,\omega e^{i\,\omega\,t^*}u^*(x^*,y^*)\right)-\frac{\mu\,\omega\,\tau}{d_1}e^{i\,\omega\,t^*}\right.$$
$$\left.\left.+\sigma\left(u^*(x^*,y^*)e^{i\,\omega\,t^*}\right)B_o^2-\sigma\left(E_0\,e^{i\,\omega\,t^*}\right)B_o-\frac{\mu}{k}\left(u^*(x^*,y^*)e^{i\,\omega\,t^*}\right)\right)\right)$$
$$=\mu\left(\left(\frac{\partial^2 u^*(x^*,y^*)}{\partial {x^*}^2}e^{i\,\omega\,t^*}+\frac{\partial^2 u^*(x^*,y^*)}{\partial {y^*}^2}e^{i\,\omega\,t^*}\right)\right.$$
$$\left.+\lambda_2\frac{\partial}{\partial t^*}\left(\frac{\partial^2 u^*(x^*,y^*)}{\partial {x^*}^2}e^{i\,\omega\,t^*}+\frac{\partial^2 u^*(x^*,y^*)}{\partial {y^*}^2}e^{i\,\omega\,t^*}\right)\right) \quad (10)$$

Dimensionless variables are defined as follows:

$$x = \frac{x^*}{d_1^*} \ , \ y = \frac{y^*}{d_1^*} \ , \ u = \frac{u^*}{d_1^* \, \omega} \ , \ \lambda = \frac{\lambda^*}{d_1^*} \ , \ \theta = \frac{\theta^*}{d_1^*} \, , \tag{11}$$

By applying the given scaling to equation (10), we can express the momentum equation in a dimensionless form.

$$(1 + \lambda_1 \omega \, i)(Re * i) \, (u) + (1 + \lambda_1 \, i\omega) \, \tau \, - (1 + \lambda_1 \omega \, i \,)(Ha)(s) + (1 + \lambda_1 \, i\omega)(Ha^2)(u) - (1 + \lambda_1 \omega i) \frac{k}{d_1^2} (u) = \, (1 + i \, \omega \lambda_2) \left(\frac{\partial^2 u}{\partial x^2} + \frac{\partial^2 u}{\partial y^2} \right), \tag{12}$$

where,

$$Ha^2 = \frac{B_o^2 \, H^2 \, \sigma_f}{\mu_f} \ , \ Ha = B_o \, H \sqrt{\frac{\sigma_f}{\mu_f}} \ , \ s = \frac{E_0}{\omega} \sqrt{\frac{\sigma_f}{\mu_f}} \ , \ Re = \frac{\rho \, \omega \, H^2}{\mu_f} \ , \ \frac{1}{Da} = \frac{d_1^2}{k},$$

and

$$\beta = \frac{(1 + \lambda_1 \, i \, \omega) \left(Re * i + Ha^2 - \frac{1}{Da} \right)}{(1 + i \, \omega \lambda_2)}$$

$$P = \frac{(1 + \lambda_1 \omega \, i \,)(Ha)(s) - (1 + \lambda_1 \, i\omega) \, \tau}{(1 + i \, \omega \lambda_2)}$$

$$\left(\frac{\partial^2 u}{\partial x^2} + \frac{\partial^2 u}{\partial y^2} \right) - (\beta) u + P = 0 \tag{13}$$

The parameters involved in the problem are Re, Ha, and s, where Re is the Reynolds number that represents the frequency of the Ac electric field, Ha is the Hartmann number that characterizes the ratio between the Lorenz force and the viscous force, and s is a non-dimensional parameter that indicates the strength of the electric field.

The respective boundary conditions are:

$$u = 0 \qquad at \qquad y_u = 1 + \varepsilon \sin(\lambda \, x) \tag{14}$$

$$u = 0 \qquad at \qquad y_L = -\alpha + \gamma \varepsilon \sin(\lambda \, x + \theta) \tag{15}$$

The boundary conditions (15) and (16) can be expressed as a Taylor series expansion around the mean wall positions $y = 1$ and $y = -\alpha$:

$$\begin{cases} u(x\,,1+\epsilon\ \sin(\lambda\,x)\,) = u(x\,,1) + \epsilon\sin(\lambda\,x)\ \dfrac{\partial u}{\partial y}(x\,,1) \\ \qquad + \dfrac{\epsilon^2}{2}\sin^2(\lambda\,x)\ \dfrac{\partial^2 u}{\partial y^2}(x\,,1) + \cdots\cdots\cdots\cdots \\ u(x\,,-\alpha\ +\gamma\ \varepsilon\ \sin(\lambda x+\theta)\,) = u(x\,,-\alpha) + \gamma\ \varepsilon\sin(\lambda x+\theta)\ \dfrac{\partial u}{\partial y}(x\,,-\alpha) \\ \qquad +\gamma^2\dfrac{\varepsilon^2}{2}\sin^2(\lambda x+\theta)\ \dfrac{\partial^2 u}{\partial y^2}(x\,,-\alpha) + \cdots \end{cases} \tag{16}$$

$$\varepsilon^o\ : \begin{cases} u_o(x\,,y)|_{y=1} = 0 \\ u_o(x\,,y)|_{y=-\alpha} = 0 \end{cases} \tag{17}$$

$$\varepsilon^1\ : \begin{cases} u_1(x\,,y)|_{y=1} = -\sin(\lambda\,x)\ \left.\dfrac{\partial u_o(x\,,y)}{\partial y}\right|_{y=1} \\ u_1(x\,,y)|_{y=-\alpha} = -\gamma\sin(\lambda x+\theta)\ \left.\dfrac{\partial u_o(x\,,y)}{\partial y}\right|_{y=-\alpha} \end{cases} \tag{18}$$

$$\varepsilon^2\ : \begin{cases} u_2(x\,,y)|_{y=1} = -sin(\lambda\,x)\ \left.\dfrac{\partial u_1(x\,,y)}{\partial y}\right|_{y=1} \\ \qquad -\dfrac{sin^2(\lambda\,x)}{2}\ \left.\dfrac{\partial^2 u_o(x\,,y)}{\partial y^2}\right|_{y=1} \\ u_2(x\,,y)|_{y=-\alpha} = -\gamma\,sin(\lambda x+\theta)\ \left.\dfrac{\partial u_1(x\,,y)}{\partial y}\right|_{y=-\alpha} \\ \qquad -\gamma^2\dfrac{sin^2(\lambda x+\theta)}{2}\ \left.\dfrac{\partial^2 u_o(x\,,y)}{\partial y^2}\right|_{y=-\alpha} \end{cases} \tag{19}$$

If there was no roughness, the velocity w would be a function of y only. However, the presence of surface roughness induces a functional variation in the *x*-direction as well.

For small values of ε, the velocity function can be expressed by a regular perturbation expansion in ε,

$$u(x\,,y) = u_o(x\,,y) + \varepsilon\, u_1(x\,,y) + \varepsilon^2 u_2(x\,,y) + \cdots\cdots\cdots\cdots \tag{20}$$

By substituting Eq. (20) into Eq. (13), we get

$$\varepsilon^0: \quad \frac{\partial^2 u_0}{\partial x^2} + \frac{\partial^2 u_0}{\partial y^2} - (\beta)\, u_0 + P = 0\,, \tag{21}$$

$$\varepsilon^1: \quad \frac{\partial^2 u_1}{\partial x^2} + \frac{\partial^2 u_1}{\partial y^2} - (\beta)\, u_1 = 0, \tag{22}$$

$$\varepsilon^2: \quad \frac{\partial^2 u_2}{\partial x^2} + \frac{\partial^2 u_2}{\partial y^2} - (\beta)\, u_2 = 0. \tag{23}$$

From Eqs. (17) and (21), we get

$$u_0(\,y) = \frac{(1 - e^{-(-1+y)\sqrt{\beta}} + e^{(1+\alpha)\sqrt{\beta}} - e^{(y+\alpha)\sqrt{\beta}})p}{(1 + e^{(1+\alpha)\sqrt{\beta}})\beta}\,. \tag{24}$$

From Eqs. (18) and (22), we have

$$u_1(x\,,y)$$

$$= -\frac{2e^{\frac{1}{2}(1+\alpha)\left(2G+\sqrt{\beta}\right)} p\gamma \mathrm{Cos}[x\lambda](-1 + \mathrm{Coth}[G(1+\alpha)])\mathrm{Sin}[\theta]\mathrm{Sinh}[G - Gy]\mathrm{Sinh}\left[\frac{1}{2}(1+\alpha)\sqrt{\beta}\right]}{\left(1 + e^{(1+\alpha)\sqrt{\beta}}\right)\sqrt{\beta}}$$

$$+ \frac{2e^{\frac{1}{2}(1+\alpha)\left(2G+\sqrt{\beta}\right)} p(-1 + \mathrm{Coth}[G(1+\alpha)])\mathrm{Sin}[x\lambda]}{\left(1 + e^{(1+\alpha)\sqrt{\beta}}\right)\sqrt{\beta}} (-\gamma \mathrm{Cos}[\theta]\mathrm{Sinh}[G - Gy] + \mathrm{Sinh}[G(y$$

$$+ \alpha)])\mathrm{Sinh}[\frac{1}{2}(1+\alpha)\sqrt{\beta}] \tag{25}$$

From Eqs. (19) and (23), we get

$$u_2(x,y) = -\frac{1}{4\left(1+e^{(1+\alpha)\sqrt{\beta}}\right)\sqrt{\beta}} e^{\frac{3}{2}(1+\alpha)\sqrt{\beta}} p\Big(-1 + \mathrm{Coth}\big[(1+\alpha)\sqrt{\beta}\big]\Big)\Big(2G\mathrm{Cosh}\left[\frac{1}{2}(1+2y+3\alpha)\sqrt{\beta}\right]\mathrm{Coth}[G(1+\alpha)] + 2G\gamma(\mathrm{Cos}[\theta] + \gamma\mathrm{Cosh}[G(1+\alpha)])\mathrm{Cosh}\left[\frac{1}{2}(-3+2y-\alpha)\sqrt{\beta}\right]\mathrm{Csch}[G(1+\alpha)] - 2G(2\gamma\mathrm{Cos}[\theta] + (1+\gamma^2)\mathrm{Cosh}[G(1+\alpha)])\mathrm{Cosh}\left[\frac{1}{2}(-1+2y+\alpha)\sqrt{\beta}\right]\mathrm{Csch}[G(1+\alpha)] + 2G\gamma\mathrm{Cos}[\theta]\mathrm{Cosh}\left[\frac{1}{2}(1+2y+3\alpha)\sqrt{\beta}\right]\mathrm{Csch}[G(1+\alpha)] + \sqrt{\beta}\gamma\mathrm{Sinh}\left[\frac{1}{2}(-3+2y-\alpha)\sqrt{\beta}\right] - \sqrt{\beta}\mathrm{Sinh}\left[\frac{1}{2}(-1+2y+\alpha)\sqrt{\beta}\right] + \sqrt{\beta}\gamma\mathrm{Sinh}\left[\frac{1}{2}(-1+2y+\alpha)\sqrt{\beta}\right] - \sqrt{\beta}\mathrm{Sinh}\left[\frac{1}{2}(1+2y+3\alpha)\sqrt{\beta}\right]\Big) + \mathrm{Sin}[2x\lambda]\frac{e^{-Hy}p}{\left(4(-1+e^{2H(1+\alpha)})\left(1+e^{(1+\alpha)\sqrt{\beta}}\right)\sqrt{\beta}\right)}(-(1 + e^{(1+\alpha)\sqrt{\beta}})\sqrt{\beta}(e^H(-1+e^{2H(y+\alpha)}) + (e^{H(2+\alpha)} - e^{H(2y+\alpha)})\gamma\mathrm{Cos}[2\theta]) + 4e^{\frac{1}{2}(1+\alpha)\left(2G+\sqrt{\beta}\right)}G((e^H + e^{H(2y+\alpha)})(-1+e^{H+H\alpha})\gamma\mathrm{Cos}[\theta] + (e^H(-1 + e^{2H(y+\alpha)}) + (e^{H(2+\alpha)} - e^{H(2y+\alpha)})\gamma^2\mathrm{Cos}[2\theta])\mathrm{Cosh}[G(1+\alpha)])(-1 + \mathrm{Coth}[G(1+\alpha)])\mathrm{Sinh}[\frac{1}{2}(1+\alpha)\sqrt{\beta}]))$$

$$+ Cos[2x\lambda]\ \frac{e^{-Hy}p}{\left(4(-1+e^{2H(1+\alpha)})\left(1+e^{(1+\alpha)\sqrt{\beta}}\right)\sqrt{\beta}\right)}\Bigg(\Big(1 + e^{(1+\alpha)\sqrt{\beta}}\Big)\sqrt{\beta}\Big(2e^H\big(-1+e^{2H(y+\alpha)}\big) + \big(e^{H(2+\alpha)} - e^{H(2y+\alpha)}\big)\gamma\mathrm{Sin}[2\theta]\Big) - 4e^{H\alpha+\frac{1}{2}(1+\alpha)\left(2G+\sqrt{\beta}\right)}\big(e^{2H} - e^{2Hy}\big)G\gamma\mathrm{Cosh}[G(1+\alpha)](-1 + \mathrm{Coth}[G(1+\alpha)])\mathrm{Sin}[\theta]\mathrm{Sinh}\left[\frac{1}{2}(1+\alpha)\sqrt{\beta}\right] - 4e^{H\alpha+\frac{1}{2}(1+\alpha)\left(2G+\sqrt{\beta}\right)}\big(e^{2H} - e^{2Hy}\big)G\gamma^2(-1 + \mathrm{Coth}[G(1+\alpha)])\mathrm{Sin}[2\theta]\mathrm{Sinh}\left[\frac{1}{2}(1 + \alpha)\sqrt{\beta}\right]\Bigg)\ , \qquad (26)$$

where, $G = \sqrt{\lambda^2+\beta}$, $0 = \sqrt{4\lambda^2+\beta}$

The Eqs. (22-24) along with their boundary conditions (17-19) discussed above, are solved precisely using the DSolve function with the assistance of the Mathematica program. The value of $u_o(y)$, $u_1(x,y)$, and $u_2(x,y)$ is obtained, and then, the overall solution for the potential equation can be deduced using equation (20).

The volume flow rate per unit channel width can be expressed as follows, where the last two integrals involve the expansion of the function w in a Taylor series around the mean wall positions. The final outcome is achieved by taking an average over one wavelength of corrugations.

$$q(x) = \int_{y_l}^{y_u} u \; dy = \int_{-\alpha}^{1} u \; dy + \int_{1}^{y_u} u \; dy + \int_{y_l}^{-\alpha} u \; dy \tag{27}$$

$$\begin{aligned} q(x) = {} & \int_{-\alpha}^{1} u_o(y)\, dy + \varepsilon \left[\int_{-\alpha}^{1} \left(u_1(x,y)\right) dy) \right] \\ & + \varepsilon^2 \left[\int_{-\alpha}^{1} \left(u_2(x,y)\right) dy) \right. \\ & + \left[\mathrm{Sin}[x\lambda] * u_1(x,y))|_{y=1} - \mathrm{Sin}[x\lambda+\theta] * u_1(x,y))|_{y=-\alpha} \right] \\ & + \left(\frac{\mathrm{Sin}[\lambda x]^2}{2} \left. \frac{\partial u_o(x,y)}{\partial y} \right|_{y=1} \right. \\ & \left. \left. - \frac{\mathrm{Sin}[\lambda x+\theta]^2}{2} \left. \frac{\partial u_o(x,y)}{\partial y} \right|_{y=-\alpha} \right) \right] \end{aligned} \tag{28}$$

The mean velocity is given by

$$\mathrm{u}_m = \frac{\lambda}{4\,\pi} \int_0^{\frac{2\,\pi}{\lambda}} q(x)\, dx = u_{0m}[1 + \varepsilon^2 \phi + O(\varepsilon^4) \cdots\cdots] \tag{29}$$

3. Discussion and Outcomes

This section investigates the behavior of gold nanofluid flowing through corrugated walls through graphical analysis. The partial differential equations were solved analytically using perturbation methods, and approximative analytical solutions were obtained using Mathematica software.

Mean velocity, flow rate, concentration, and heat transfer rate were examined at various locations in the microchannel. In order to verify the accuracy of the results, Table 2

compares the obtained results with previously published data obtained under identical conditions, at $\alpha = 0, \tau = 0.5, \lambda = 0.1, Re = 0, s = 0, \lambda_1 = \lambda_2 = 0$ and $\varepsilon = 0.1, \alpha = 1, \gamma = 1$. It should be noted that the microfluid analysis assumes the channel's half-height to be $H \sim 40\ \mu m$. The following primary parameter values were utilized to study the impacts of corrugated nanofluid flow [24].

$$O(\rho) \sim 1 \times 10^3 - 5.91 \times 10^3\ kg\ m^{-3}, O(\mu) \sim 0.001\ kg\ ms^{-1},$$
$$O(By) \sim 1 - 50T, O(Ex)\ 0 - 10^4\ V\ m^{-1}, O(Ez) \sim 0 - 10^4\ V\ m^{-1}$$

Table 1: Comparison of numerical values of volumetric flow rate for different Hartmann number (Ha)

Ha	A. Y. Sayed *et al.* [2023]		Present work	
	$q(1)$	$q(60)$	$q(1)$	$q(60)$
0	0.333672	0.331201	0.333691	0.331198
0.1	0.332354	0.329813	0.332362	0.329877
0.5	0.303385	0.301087	0.303397	0.301090
1	0.238672	0.236752	0.238688	0.236783

Table 2: Typical values of the physical variables [24]

Physical variables	Values [units]
Characteristic channel length (H)	$40\ \mu m$
Electrical field in axial direction (E_x)	$0 - 2 \times 10^4\ V/m$
Applied magnetic field (B_y)	$1 - 50\ T$
Viscosity of the fluid (μ)	$10 - 6\ m^2/s$
Electrical conductivity (σ_e)	$1000\ W/m^2$

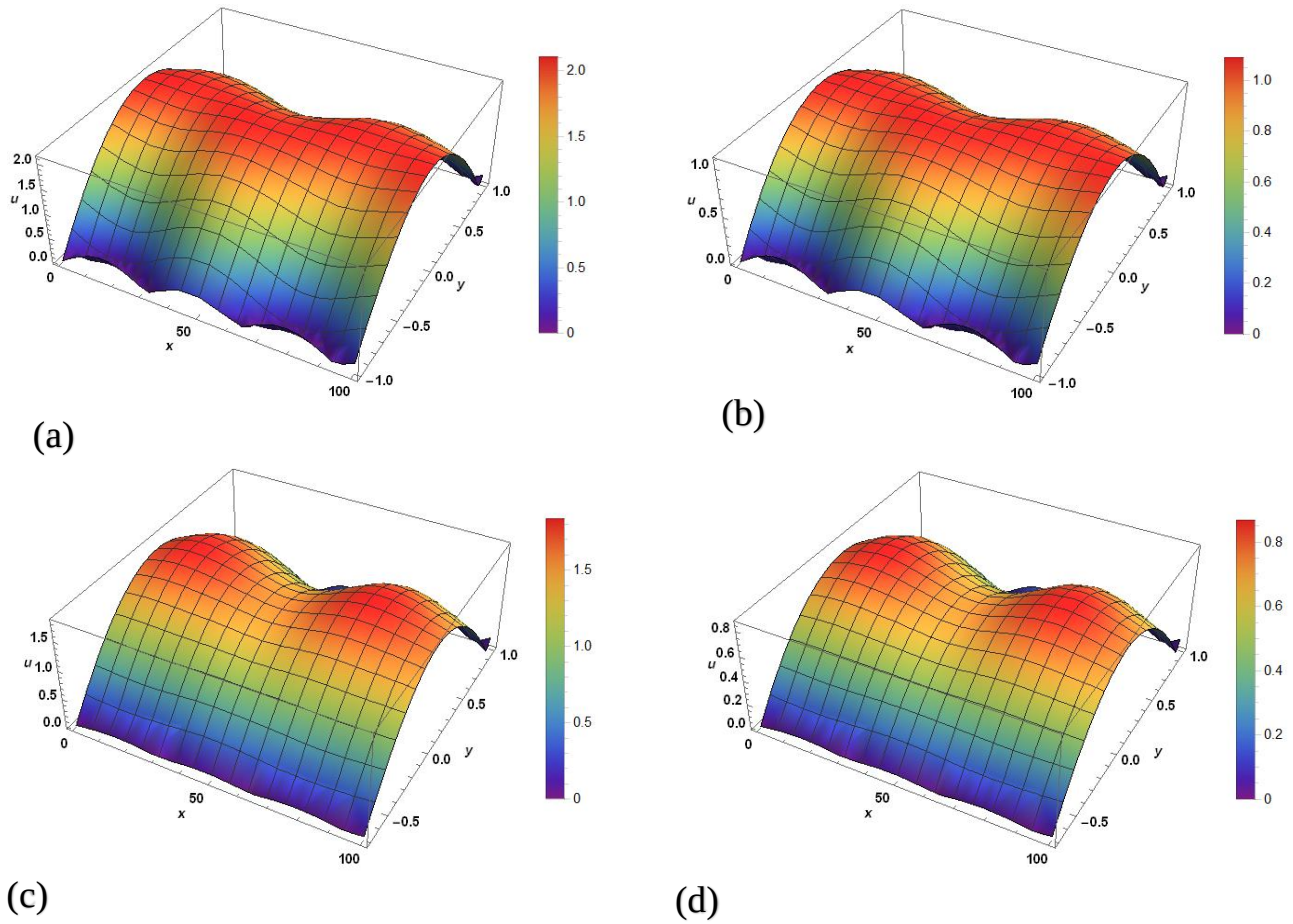

Figure 2. The velocity distribution in three dimensions for $\varepsilon = 0.1$, $\lambda = 0.1$, $Ha = 0.5, s = 10, \omega = \pi, \tau = 1$, $\theta = 0, Da = 0.2, Re = 0.5, \alpha = 1, \gamma = 1.$ (a) Symmetric $\lambda_1 = 0.1, \lambda_2 = 0.5$ (b) Symmetric $\lambda_1 = 0.1, \lambda_2 = 1$(c) Asymmetric $\lambda_1 = 0.1, \lambda_2 = 0.5, \alpha = 0.7$, $\gamma = 0.2$ (d) Asymmetric $\lambda_1 = 0.1, \lambda_2 = 1, \alpha = 0.7$, $\gamma = 0.2$

In the case of a symmetric and asymmetric corrugated channels where $\theta = 0$, as seen in figures (2a-d) and contour plots (3a-d), the velocity of the Jeffrey fluid decreases with increasing retardation time due to the longer time required for the fluid molecules to relax.

The presence of corrugated walls in the channel causes additional flow resistance, exacerbating the velocity reduction in non-Newtonian fluids compared to Newtonian fluids with constant viscosity.

This effect is particularly pronounced at lower values of the retardation time when the fluid has less time to adapt to the changing channel geometry.

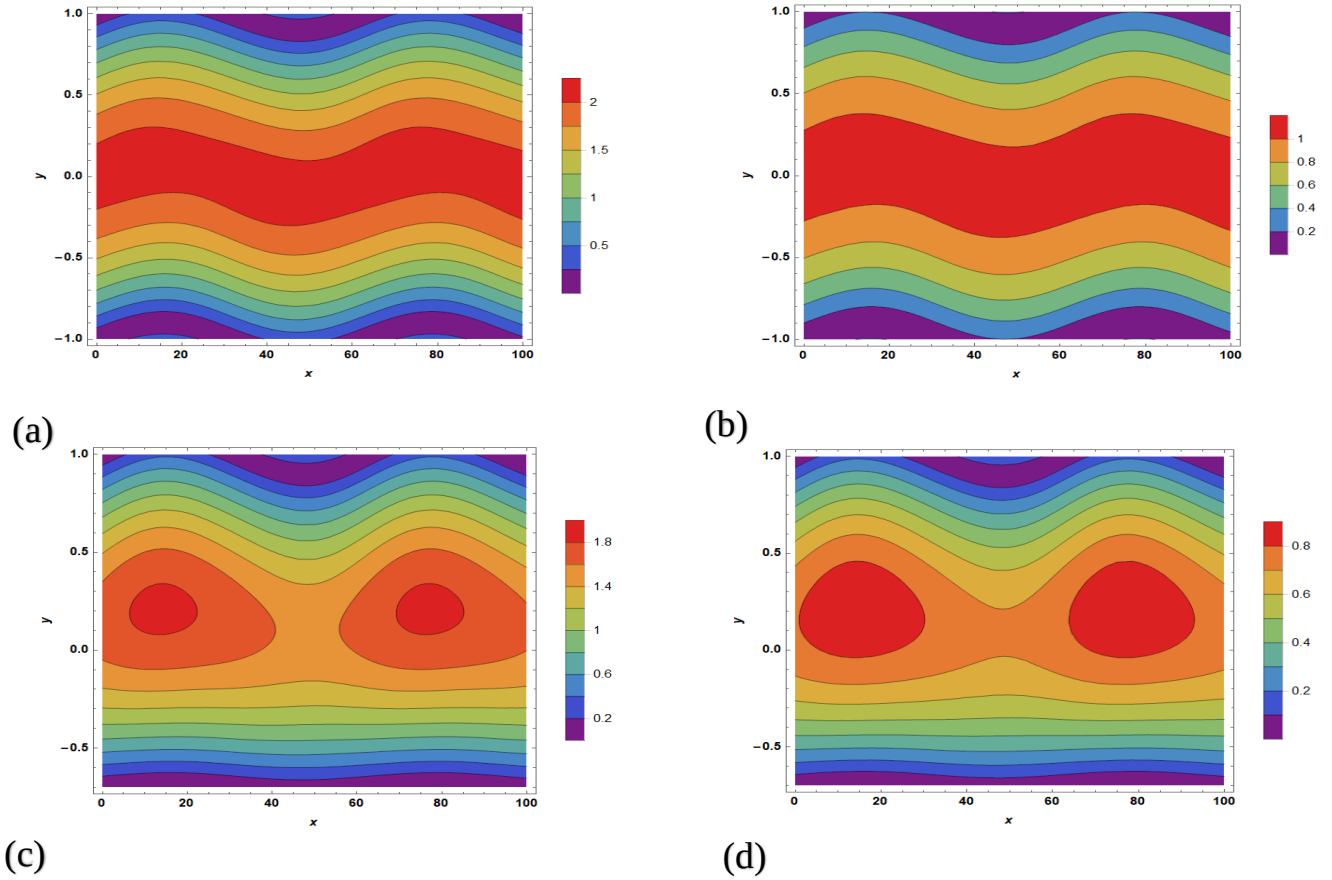

Figure 3. Contour plot for velocity distribution $\varepsilon = 0.1, \lambda = 0.1, Ha = 0.5, s = 10, \omega = \pi, \tau = 1, \theta = 0, Da = 0.2, Re = 0.5, \alpha = 1, \gamma = 1.$ (a) Symmetric $\lambda_1 = 0.1, \lambda_2 = 0.5$ (b) Symmetric $\lambda_1 = 0.1, \lambda_2 = 1$(c) Asymmetric $\lambda_1 = 0.1, \lambda_2 = 0.5, \alpha = 0.7, \gamma = 0.2$ (d) Asymmetric $\lambda_1 = 0.1, \lambda_2 = 1, \alpha = 0.7, \gamma = 0.2$

Figures (4a-d) and contour plots (5a-d) show that the corrugated walls of the channel also create additional flow resistance, leading to a reduction in the velocity of the non-Newtonian fluid.

However, in this case, the value of $\theta = \pi$, causing the top and bottom walls to be symmetric with respect to the channel centerline.

This symmetry can result in a more uniform flow profile, which may explain the smaller decrease in velocity with increasing retardation time compared to the previous case.

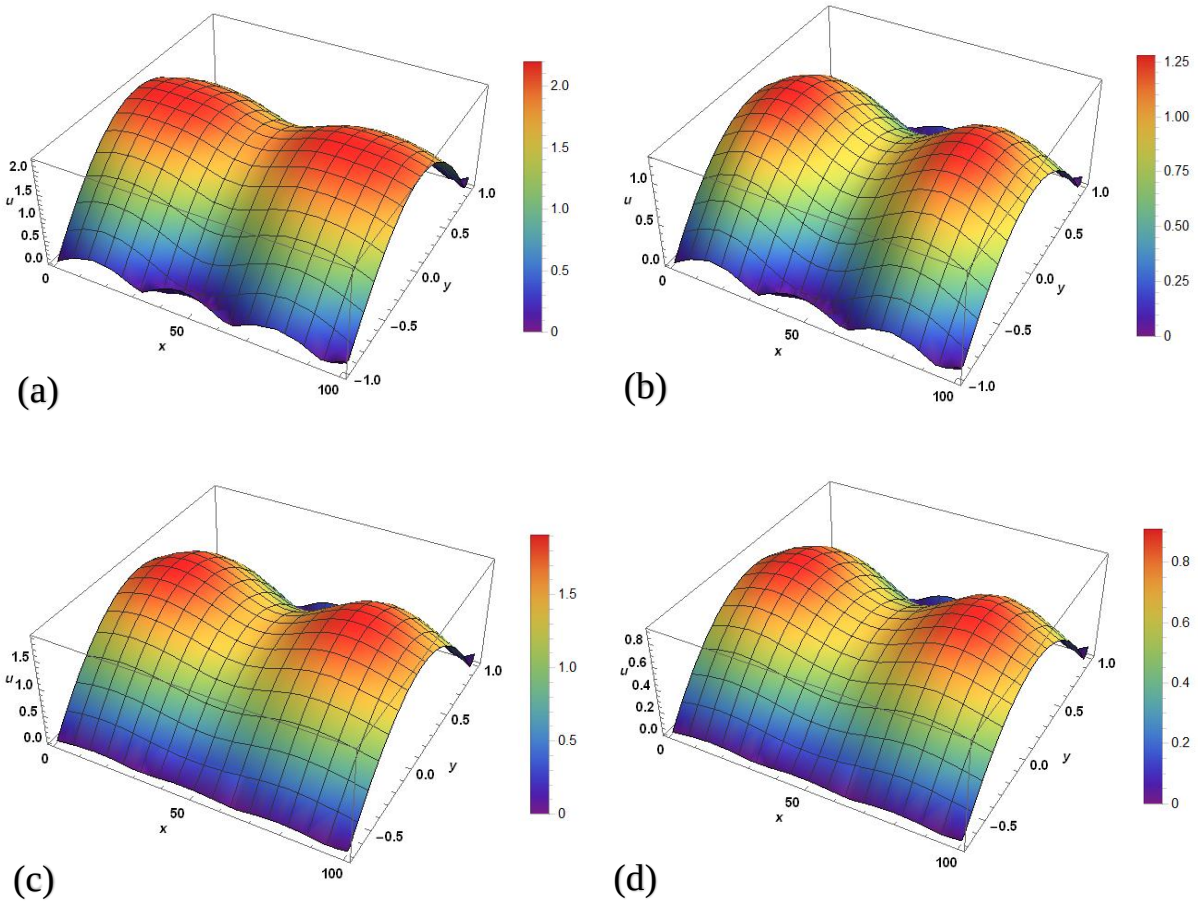

Figure 4. The velocity distribution in three dimensions for $\varepsilon = 0.1$, $\lambda = 0.1$, $Ha = 0.5, s = 10, \omega = \pi, \tau = 1$, $\theta = \pi, Da = 0.2, Re = 0.5, \alpha = 1, \gamma = 1$. (a) Symmetric $\lambda_1 = 0.1, \lambda_2 = 0.5$ (b) Symmetric $\lambda_1 = 0.1, \lambda_2 = 1$(c) Asymmetric $\lambda_1 = 0.1, \lambda_2 = 0.5, \alpha = 0.7$, $\gamma = 0.2$ (d) Asymmetric $\lambda_1 = 0.1, \lambda_2 = 1, \alpha = 0.7$, $\gamma = 0.2$

In Figure (6), it can be observed that the velocity of the non-Newtonian fluid is lower than that of the Newtonian fluid in the symmetric case, as well as in the asymmetric case.

This can be explained by the fact that the corrugated channel geometry creates additional flow resistance for the non-Newtonian fluid, leading to a reduction in its velocity. In the symmetric case, the flow profile is more uniform due to the symmetry of the channel, resulting in less resistance to flow and a smaller decrease in velocity.

However, even with this more uniform flow profile, the non-Newtonian fluid still experiences a larger decrease in velocity compared to the Newtonian fluid due to its non-linear viscosity.

In the asymmetric case, the flow profile is less uniform, resulting in more resistance to flow and a larger decrease in velocity for both the Newtonian and non-Newtonian fluids.

In summary, the presence of corrugations in the channel creates additional flow resistance, which leads to a reduction in the velocity of both Newtonian and non-Newtonian fluids.

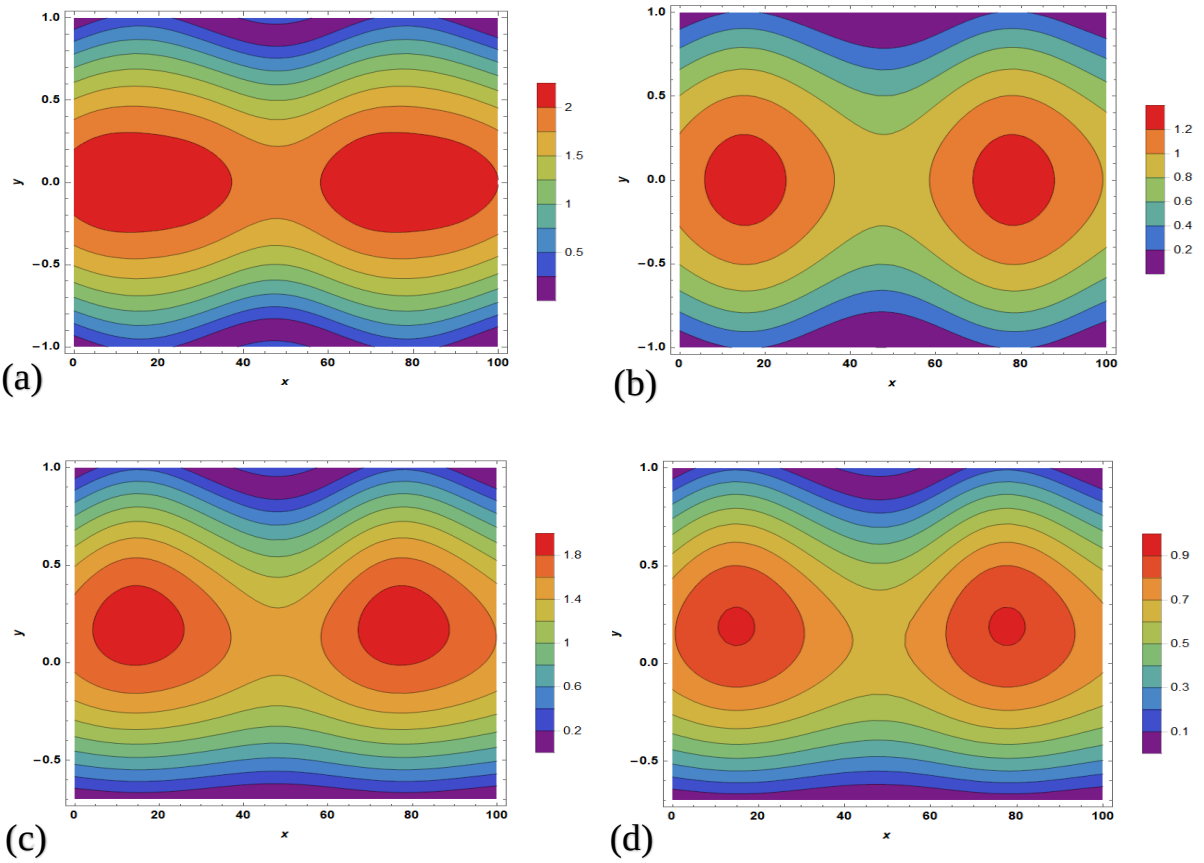

Figure 5. Contour plot for velocity distribution for $\varepsilon = 0.1$, $\lambda = 0.1$, $Ha = 0.5, s = 10, \omega = \pi, \tau = 1$, $\theta = \pi, Da = 0.2, Re = 0.5, \alpha = 1, \gamma = 1$. (a) Symmetric $\lambda_1 = 0.1, \lambda_2 = 0.5$ (b) Symmetric $\lambda_1 = 0.1, \lambda_2 = 1$(c) Asymmetric $\lambda_1 = 0.1, \lambda_2 = 0.5, \alpha = 0.7$, $\gamma = 0.2$ (d) Asymmetric $\lambda_1 = 0.1, \lambda_2 = 1, \alpha = 0.7$, $\gamma = 0.2$

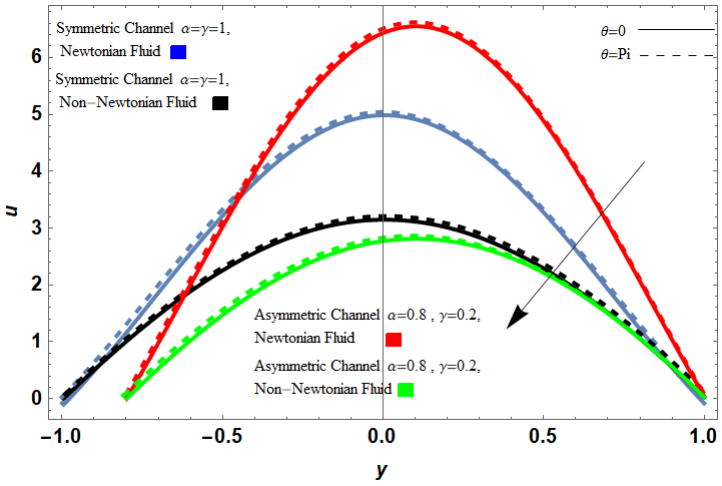

Figure 6. The velocity distribution with Symmetric and Asymmetric Channels for a prescribed value of $x = 0.5\ \ \varepsilon = 0.1, \lambda = 0.1, s = 10, \tau = 2, \omega = \pi, \lambda_1 = 0.1, \lambda_2 = 0.5, Re = 1, \tau = 2, Da = 0.2$

In Figure (7). As the Hartmann number was increased from 0 to 2, the velocity of the non-Newtonian fluid increased. This is because the magnetic field exerts a force on the fluid that enhances the flow in the direction perpendicular to the magnetic field lines. However, as the Hartmann number was further increased beyond 2, the velocity of the non-Newtonian fluid started to decrease. This is because the magnetic field became strong enough to suppress the fluid motion and dampen the flow. The value of the relaxation time is relatively low, indicating that the fluid has less time to adapt to the changing geometry of the channel. However, increasing the value

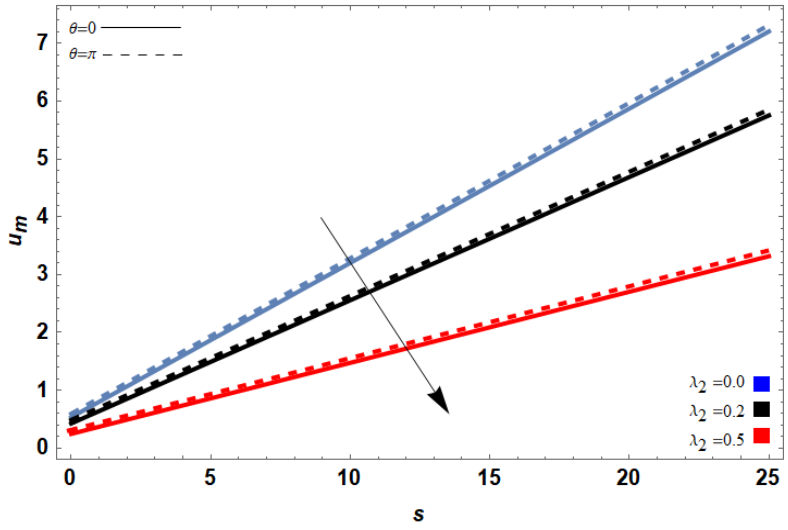

Figure 7. The mean velocity with Hartmann number (Ha) for $\varepsilon = 0.1, \lambda = 0.1, s = 10, \tau = 2, \omega = \pi, \lambda_1 = 0.1, Re = 1, \tau = 2, \alpha = 1, \gamma = 1, Da = \infty$

of the retardation time (0.1 to 0.3) led to an increase in the fluid velocity. This is because the retardation time controls the rate at which the fluid molecules resist deformation, and increasing the retardation time allows the fluid to better adapt to the changing channel geometry, resulting in a more efficient flow.

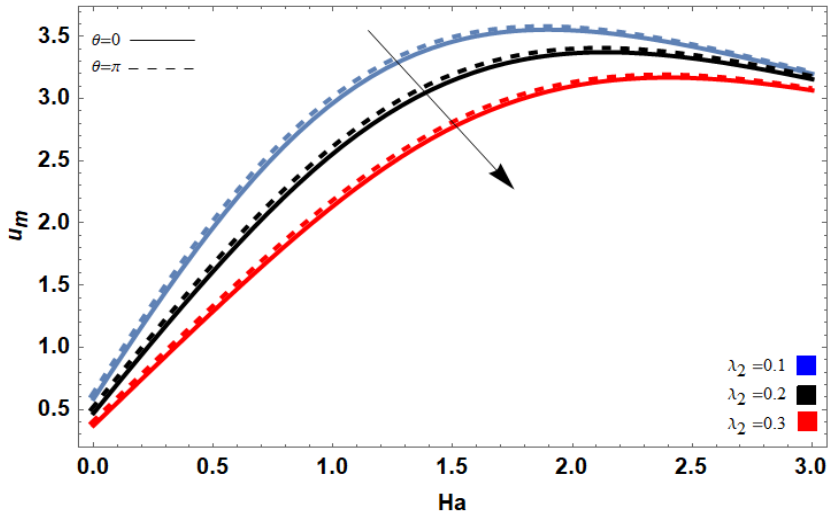

Figure 8. The mean velocity with Electric field (s) for $\varepsilon = 0.1, \lambda = 0.1, s = 10, \tau = 2, \omega = \pi, \lambda_1 = 0.1, Re = 1, \tau = 2, \gamma = 1, Da = \infty$

As shown in Figure (9), the velocity of the non-Newtonian fluid increased for all the values of retardation time (0, 0.5) as the 0.2, and field electric strength

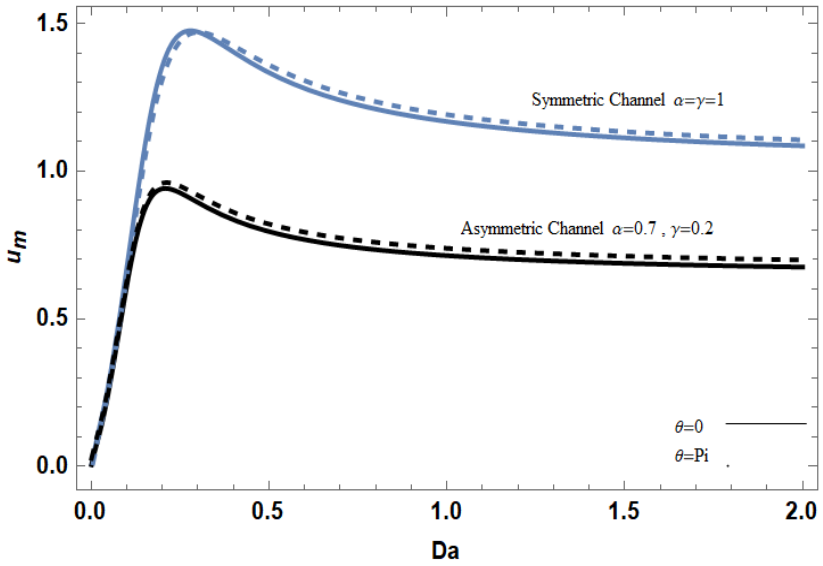

was increased from 0 to 25. This is because the electric field exerts a force on the fluid that enhances the flow in the direction perpendicular to the electric field lines. The magnitude of the increase in velocity varies with the value of the retardation time and decreases as the value of the retardation time increases. This is because the retardation time controls the rate at which the fluid molecules resist deformation, and a higher retardation time means that the fluid resists the electric field force more strongly, leading to a smaller increase in velocity.

Figure 9. The mean velocity with Porous medium (Da) for $\varepsilon = 0.1$, $\lambda = 0.1$, $s = 10, \tau = 2, \omega = \pi, \lambda_1 = 0.1, \lambda_2 = 0.5, Re = 0.5$

In Figure 9, the relationship between the mean velocity and the porous medium for the non-Newtonian fluid is shown. It can be observed that the mean velocity increases from zero to approximately 0.3, then decreases slightly before stabilizing. Furthermore, the mean velocity in the symmetric channel is greater than that in the asymmetric channel. This behavior can be explained by the presence of the porous medium, which creates additional resistance to flow.

As the fluid flows through the porous medium, it experiences more resistance compared to a smooth channel due to the presence of the solid particles. This resistance leads to a decrease in mean velocity.

However, as the fluid flows further downstream, it begins to recover some of its velocity due to the reduction in solid particle concentration. This is why the mean velocity increases initially before reaching a peak and then decreasing slightly before stabilizing. The difference in mean velocity between the symmetric and asymmetric channels can be attributed to the difference in flow profile.

In the symmetric case, the flow is more uniform, resulting in less resistance to flow and a higher mean velocity. In contrast, in the asymmetric case, the flow is less uniform, resulting in more resistance to flow and a lower mean velocity.

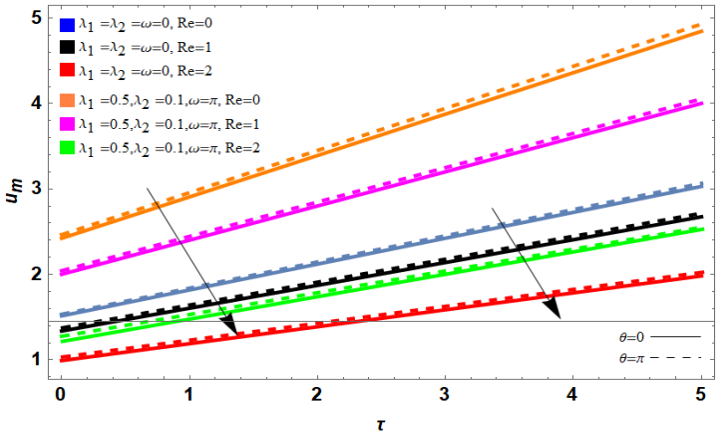

Figure 10. The mean velocity with Amplitude pulsating pressure (τ) for $\varepsilon = 0.1$, $\lambda = 10, \omega = \pi, \lambda_1 = 0.1, s = 0.1, \lambda_2 = 0.5, Re = 0.5, Da = \infty$

In Figure (10), as the Reynolds number was increased from 0 to 2, the velocity of the non-Newtonian fluid decreased. This is because the flow became more turbulent at higher Reynolds numbers, which increased the flow resistance and decreased the fluid velocity. The parameters used were Retardation time $\lambda_2 = 0.5$, Relaxation time $\lambda_1 = 0.1$, and Angular frequency $\omega = \pi$. The Reynolds number was varied at values of 0, 1, and 2. At these parameter values, the velocity of the non-Newtonian fluid decreased as the Reynolds number was increased. This is due to the increase in flow resistance associated with higher Reynolds numbers, as previously mentioned.

The value of the angular frequency of the pulsating pressure is $\omega = \pi$, which corresponds to a half-period of the sine wave. This may result in a more uniform flow profile and smaller decrease in velocity with increasing Reynolds number compared to cases where the angular frequency is different.

4. Conclusion.

This study investigates the behavior of non-Newtonian fluids, specifically Jeffery fluids, in both symmetric and asymmetric corrugated channels under different external influences. Non-Newtonian fluids exhibit distinct flow behaviors in comparison to Newtonian fluids and are frequently encountered in various engineering applications. Understanding their behavior in complex geometries, such as corrugated channels, is crucial for designing and optimizing these applications.

The study focuses on the behavior of non-Newtonian Jeffery fluids in a corrugated channel under different external influences.

- Corrugated channels and porous media create additional flow resistance, leading to a reduction in velocity and mean velocity of non-Newtonian fluids.
- Non-Newtonian fluids experience larger decreases in velocity compared to Newtonian fluids due to their non-linear viscosity.
- Channel asymmetry can result in a less uniform flow profile, leading to more resistance to flow and a larger decrease in velocity compared to symmetric channel geometry.
- The presence of a porous medium also creates additional resistance to flow, leading to a decrease in mean velocity for the non-Newtonian fluid.
- Understanding the behavior of non-Newtonian fluids in complex geometries is crucial for the design and optimization of fluid systems in various engineering applications, including chemical processing, biomedical devices, and microfluidic devices.

Declarations

- **Competing interests**: The authors declare that they have no competing interests.

- **Funding**: Not applicable.

- **Ethical approval**: This article does not contain any studies with human participants or animals performed by any of the authors.

Acknowledgements
We express our gratitude to the anonymous referees for their constructive reviews of the manuscript and for helpful comments.

References.

[1]Stone H A, Stroock A D and Ajdari A 2004 Engineering flows in small devices microfluidics toward a lab-on-a-chip Ann. Rev. Fluid Mech. 36 381

[2] Singhal V, Garimella S V and Ramam A 2004 Microscale pumping technologies for microchannel cooling system Appl. Mech. Rev. 57 191

[3] Sviridov V G, Ivochkin Yu P, Razuvanov N G, Zhilin V G, Genin L G, Ivanova O N and Averianov K V 2003 Liquid metal MHD heat transfer investigations applied to fusion tokamak reactor cooling ducts Magnetohydrodynamics 39 557

[4] Abhari F, Jaafar H and Yunus N A M 2012 A comprehensive study of micropumps technologies Int. J. Electrochem. Sci. 7 9765

[5] Lemoff A V and Lee A P 2000 An ac magnetohydrodynamic micropump Sensors Actuators B 63 178

[6] Nguyen N T and Kassegne S K 2008 High-current density dc magenetohydrodynamics micropump with bubble isolation and release system Microfluid. Nanofluidics 5 383

[7] Xie Z Y and Jian Y J 2014 Rotating electroosmotic flow of power-law fluids at high zeta potential Colloid Surf. A: Physicochem. Eng. Asp. 461 231

[8] Jian Y J, Yang L G and Liu Q S 2010 Time periodic electroosmotic flow through a microannulus Phys. Fluids 22 042001

[9] S. Nadeem and E.N. Maraj, Commun. Theor. Phys. 59 (2013) 729.

[10] G.F.K. Tay, D.C.S. Kuhn, and M.F. Tachie, Int. J. Heat Fluid Fl. 30 (2009) 249.

[11] J.M. Tsikata and M.F. Tachie, Int. J. Heat Fluid Fl. 44 (2013) 239.

[12] J.M. Tsikata and M.F. Tachie, Int. J. Heat Fluid Fl. 39 (2013) 127.

[13] Buren M, Jian Y J and Chang L 2014 Electromagnetohydrodynamic flow through a microparallel channel with corrugated walls J. Phys. D: Appl. Phys. 47 425501

[14] Tsougenia K, Petroub P S, Papageorgioua D P, Kakabakosb S E, Tserepia A and Gogolidesa E 2012 Controlled protein adsorption on microfluidic channels with engineered roughness and wettability Sensors Actuators B 161 216

[15] Huang Y G, Liu S B, Yang W and Yu C X 2010 Surface roughness analysis and improvement of PMMA- based microfluidic chip chambers by CO2 laser cutting Appl. Surf. Sci. 256 1675

[16] Riaz A, Nadeem S, Ellahi R and Zeeshan A 2014 Exact solution for peristaltic flow of Jeffrey fluid model in a threedimensional rectangular duct having slip at the walls Appl. Bionics Biomech. 11 81

[17] Khan A A, Ellahi R and Vafai K 2012 Peristaltic transport of a jeffrey fluid with variable viscosity through a porous medium in an asymmetric channel Adv. Math. Phys. 2012 15

[18] Bird R B, Stewart W E and Lightfoot E N 2001 Transport Phenomena 2nd edn (New York: Wiley)

[19] Liu Q S, Jian Y J and Yang L G 2011 Alternating current electroosmotic flow of the Jeffreys fluids through a slit microchannel Phys. Fluids 23 102001

[20] Gao Y D, Wong T N, Yang C and Ooi K T 2005 Two–fluid electroosmotic flow in microchannels J. Colloid Interface Sci. 284 306

[21] D. Si and Y. Jian, J. Phys. D: Appl. Phys. 48 (2015) 085501.

[22] M. Buren, Y. Jian, and L. Chang, J. Phys. D: Appl. Phys.47 (2014) 425501.

[23] M. Buren and Y. Jian, Electrophoresis 36 (2015) 1539.

[24] A. Y. Sayed, S. I. Ahmed, K. S. Mekheimer, and M. S. Abdel-wahed, “Electromagnetohydrodynamic effects with single-walled carbon nanotubes particles in a corrugated microchannel,” Chaos, Solitons Fractals Interdiscip. J. Nonlinear Sci. Nonequilibrium Complex Phenom., vol. 168, no. December 2022, p. 113126, 2023, doi: 10.1016/j.chaos.2023.113126.

[25] R. Ellahi, M. Hassan, A. Zeeshan, A.A. Khan, The shape effects of nanoparticles suspended in HFE-7100 over wedge with entropy generation and mixed convection, Applied Nanoscience, 6(2016), pp.641-651.

[26] M. Sheikholeslami, Numerical approach for MHD Al2O3-water nanofluid transportation inside a permeable medium using innovative computer method, Computer Methods in Applied Mechanics and Engineering 344 (2019) 306–318.

[27] Zahir Shah , Arshad Khan , Waris Khan , M. Kamran Alam , Saeed Islam , Poom Kumam , Phatiphat Thounthong, Micropolar Gold Blood Nanofluid flow and Radiative Heat Transfer between Permeable Channels, Journal Pre-proof, Biomedicine (2019), doi: https://doi.org/10.1016/j.cmpb.2019.105197

[28] Dongqing Si and Yongjun Jian, Electromagnetohydrodynamic (EMHD) micropump of Jeffrey fluids through two parallel microchannels with corrugated walls, J. Phys. D: Appl. Phys. 48 (2015) 085501 (10pp), doi:10.1088/0022-3727/48/8/085501.

[29] Yu-Fei Wei, Hai-Jun Wang and Yong-Jun Jian, Pressure Oscillating Flow in Corrugated Parallel Channel, Chinese Physical Society and IOP Publishing Ltd, Volume 66, Number 6DOI 10.1088/0253-6102/66/6/694.

[30] Sayed, A.Y., Abdel-wahed, M.S. Entropy analysis for an MHD nanofluid with a microrotation boundary layer over a moving permeable plate. Eur. Phys. J. Plus 135, 106 (2020). https://doi.org/10.1140/epjp/s13360-020-00181-6